Available online at www.sciencedirect.com
SCIENCE DIRECT®
International Journal of Thermal Sciences 44 (2005) 865–878
International Journal of Thermal Sciences
www.elsevier.com/locate/ijts

Natural convection in cavities with constant flux heating at the bottom wall and isothermal cooling from the sidewalls

Muhammad A.R. Sharif *, Taquiur Rahman Mohammad

Aerospace Engineering and Mechanics Department, The University of Alabama, Tuscaloosa, AL 35487-0280, USA

Received 24 May 2004; received in revised form 10 February 2005; accepted 14 February 2005

Available online 14 April 2005

Abstract

Natural convection in rectangular cavities is studied numerically using a finite volume based computational procedure. In many applications, especially for cooling of electronic components, a natural convection configuration is encountered where a constant flux heating element at the bottom surface are cooled from the isothermal sidewalls while the top wall can be considered adiabatic. The present study is based on such a configuration where a constant flux heat source is symmetrically embedded at the bottom wall. The length of the heat source is varied from 20 to 80% of the total length of the bottom wall. The non-heated parts of the bottom wall are considered adiabatic. The Grashof number is varied from 10^3 to 10^6. The study includes computations for cavities at various aspect ratios, ranging from 0.5 to 2, and inclination angles of the cavity from 0° to 30°. The effects aspect ratio, inclination angles, and heat source length on the convection and heat transfer process in the cavity are analysed. Results are presented in the form of streamline and isotherm plots as well as the variation of the Nusselt number and maximum temperature at the heat source surface under different conditions.

Keywords: Numerical heat transfer; Rectangular enclosure; Natural convection; Aspect ratio; Electronic component cooling

1. Introduction

Air-cooling is one of the preferred methods for cooling computer systems and other electronic equipment, due to its simplicity and low cost. The electronic components are treated as heat sources embedded on flat surfaces [1]. In many applications natural convection is the only feasible mode of cooling of the heat source. Besides cooling of the electronic components, there are numerous other practical applications of natural convective cooling in rectangular enclosures with various combinations of the temperature gradients, cavity aspect ratios, placement of the heat source and cold surfaces, etc.

The problem of convective heat transfer in an enclosure has been studied extensively because of the wide application of such process. Ostrach [2] provided a comprehensive review article and extensive bibliography on natural convection in cavities up to 1988. Other articles on the topic published after 1988 include Valencia and Frederick [3], Selamet et al. [4], Hasnaoui et al. [5], Papanicolaou and Gopalakrishna [6], Sundstrom and Kimura [7], Hsu and Chen [8], Elsherbiny et al. [9], and Nguyen and Prudhomme [10], among others, who investigated natural convection in rectangular enclosures under various configurations and orientations.

Majority of the published studies on natural convection in rectangular cavities considered either vertically or horizontally imposed temperature gradient. For vertically imposed temperature gradient the heat source is at the bottom surface of the cavity and the top surface being at a colder temperature. The sidewalls are considered adiabatic. On the other hand for horizontal temperature gradient the heat source is on one of the sidewall while the other sidewall is maintained at a colder temperature. The top and bottom surfaces are considered adiabatic. The hot walls in these configurations may be either of isothermal type or constant heat flux type.

* Corresponding author. Tel.: +205 348 8052; fax: +205 348 7240.
E-mail address: msharif@coe.eng.ua.edu (M.A.R. Sharif).

1290-0729/$ – see front matter
doi:10.1016/j.ijthermalsci.2005.02.006

Nomenclature

A	aspect ratio of the cavity, H/W	V	dimensionless velocity component in y-direction
g	gravitational acceleration ..... $m\,s^{-2}$	W	width of the enclosure ..... m
Gr	Grashof number	*Greek symbols*	
H	height of the enclosure ..... m	α	thermal diffusivity ..... $m^2 \cdot s^{-1}$
k	thermal conductivity of air ..... $W \cdot m^{-1} \cdot K^{-1}$	β	thermal expansion coefficient ..... K^{-1}
L	length of the heat source ..... m	γ	cavity inclination angle
P	dimensionless local pressure	θ	dimensionless temperature
Pr	Prandtl number	ν	kinematic viscosity ..... $m^2 \cdot s^{-1}$
q''	heat flux at the source ..... $W \cdot m^{-2}$	ε	dimensionless length of the heat source, L/W
T	temperature ..... K		
U	dimensionless velocity component in x-direction		

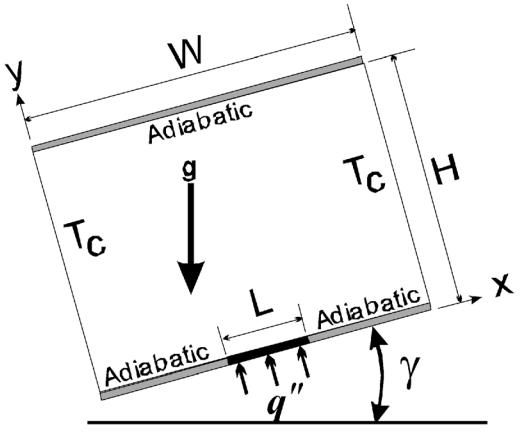

Fig. 1. Schematic diagram of the physical system.

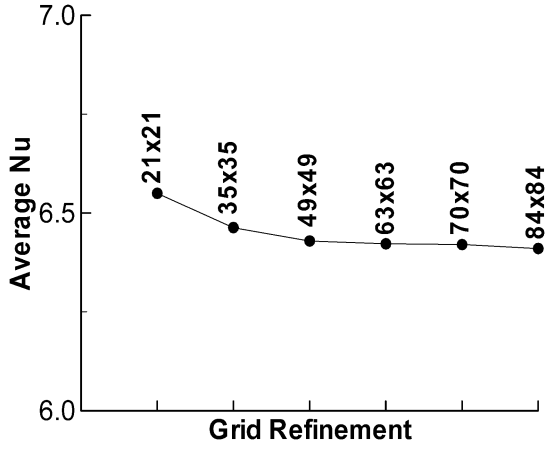

(a)

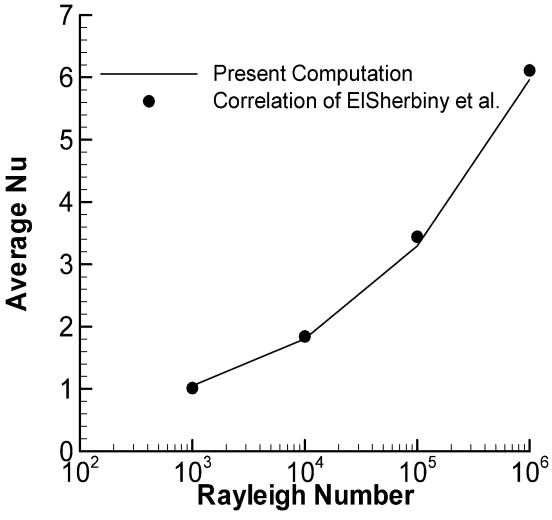

(b)

Fig. 2. (a) Convergence of the average Nusselt number with grid refinement, (b) comparison of the present computation with the experimental correlation of Elsherbiny et al.

In many applications, especially for cooling of electronic components, a configuration is encountered where the heat source is at the bottom surface but the sidewalls are at the colder temperature while the top wall can be considered adiabatic. There have been relatively few studies involving natural convection in similar configurations published in the past. Anderson and Lauriat [11] studied the natural convection in a vertical square cavity heated from bottom and cooled from one side. They observed a single cell flow pattern and the absence of Benard type instabilities. Convection in a similar configuration where the bottom wall of the rectangular cavity was partially heated with cooling from one side was studied by November and Nansteel [12]. It was reported that the heated fluid layer near the bottom wall remains attached up to the turning corner. Ganzarolli and Milanez [13] performed numerical study of steady natural convection in rectangular enclosures heated from below and symmetrically cooled from the sides. The size of the cavity was varied from square to shallow where the cavity width was varied from 1–10 times of the height. The heat source, which spanned the entire bottom wall, was either isothermal or at constant heat flux condition. They observed that, for the square cavity, the flow and thermal fields are not strongly affected by the isothermal or constant heat flux boundary condition at the bottom heat source. However, distinct differences were observed between the isothermal and constant heat flux conditions for shallow cavity. For isothermal heat source condition, the cavity is not always thermally active along its whole length and the flow does not fill the cavity

uniformly. For constant heat flux condition, the isotherms and streamlines occupy the whole cavity more uniformly, even for low values of the Rayleigh number. The flow structure was found to consist of a single counter-clockwise cell for all cases studied, except for a small secondary cell due to viscous drag in some cases for isothermal condition at the bottom wall of the cavity. More recently, Aydin and Yang [14] numerically investigated the natural convection of air in a vertical square cavity with localized isothermal heating from below and symmetrical cooling from the sidewalls. The top wall as well as the non-heated parts of the bottom wall was considered adiabatic. The length of the symmetrically placed isothermal heat source at the bottom was varied. Two counter rotating vortices were formed in the flow domain due to natural convection. The average Nusselt number at the heated part of the bottom wall was shown to increase with increasing Rayleigh number as well as with increasing length of the heat source.

The present study is based on the configuration of Aydin and Yang [14] where the localized isothermal heat source at the bottom wall is replaced with a constant flux heat source, which is physically more realistic for electronic component cooling applications. Aydin and Yang [14] did not investigate the effect of aspect ratio and inclination of the cavity on the heat transfer process. Ganzarolli and Milanez [13] also considered similar configuration and boundary conditions but their heat source spanned the entire bottom wall instead of being localized and they only considered square to shallow enclosures leaving out the cases for tall enclosures when the height is larger than the width.

The physical model considered here is shown in Fig. 1, along with the important geometric parameters. It consists of a rectangular cavity of dimension, $W \times H$, whose sidewalls are kept at a constant temperature, T_C. The aspect ratio of the cavity is defined as $A = H/W$. The bottom wall has an embedded symmetrical heat source with constant heat flux, q'', and length L. The remaining parts of the bottom wall and the entire upper wall are adiabatic. With this geometry and boundary conditions, the present study reports the computations for cavities at various aspect ratios, ranging from 0.5 to 2, and inclination angles from 0° to 30°, and their effects on the heat transfer process is analysed and the results are presented in terms of the variation of the average Nusselt number and maximum temperature at the heat source surface. The natural convection parameter, Grashof number is varied from 10^3 to 10^6. Another important parameter of investigation is the ratio of the heating element to the cavity width, L/W, which is subsequently designated as ε and is varied from 0.2 to 0.8.

2. Mathematical formulation

The governing equations for laminar steady convection, after invoking the Boussinesq approximation and neglecting the viscous dissipation, can be expressed in the dimensionless form as

$$\frac{\partial U}{\partial X} + \frac{\partial V}{\partial Y} = 0 \tag{1}$$

$$U\frac{\partial U}{\partial X} + V\frac{\partial U}{\partial Y} = -\frac{\partial P}{\partial X} + \left(\frac{\partial^2 U}{\partial X^2} + \frac{\partial^2 U}{\partial Y^2}\right) + (Gr\sin\gamma)\theta \tag{2}$$

$$U\frac{\partial V}{\partial X} + V\frac{\partial V}{\partial Y} = -\frac{\partial P}{\partial Y} + \left(\frac{\partial^2 V}{\partial X^2} + \frac{\partial^2 V}{\partial Y^2}\right) + (Gr\cos\gamma)\theta \tag{3}$$

$$U\frac{\partial \theta}{\partial X} + V\frac{\partial \theta}{\partial Y} = \frac{1}{Pr}\left(\frac{\partial^2 \theta}{\partial X^2} + \frac{\partial^2 \theta}{\partial Y^2}\right) \tag{4}$$

where U and V are the velocity components in the X and Y directions, respectively, P is the pressure, θ is the temperature, and γ is the inclination angle of the cavity with the horizontal direction. Here, all distances are normalized by W, all velocities are normalized by ν/W, and pressure is normalized by $\rho(\nu/W)^2$; ρ and ν being the fluid density and kinematic viscosity, respectively. The cavity width W is chosen for normalizing the distances since the dimensions H and L are varied while keeping W fixed for varying the aspect ratio, A, and the normalized heat source length, ε. The temperature is normalized as $\theta = (T - T_C)/\Delta T$ where ΔT is the temperature scaling defined as $q''W/k$; k being the thermal conductivity of the fluid. The dimensionless parameters appearing in Eqs. (2)–(4) are the Prandtl number $Pr = \nu/\alpha$ and the Grashof number $Gr = g\beta\Delta T W^3/\nu^2$, where α is the thermal diffusivity of the fluid, β is the thermal expansion coefficient of the fluid, and g is the gravitational acceleration.

The boundary conditions for the present problem is specified as follows:

Top wall:

$$U = V = 0, \qquad \partial\theta/\partial Y = 0$$

Bottom wall:

$$U = V = 0$$

$$\partial\theta/\partial Y = \begin{cases} 0, & \text{for } 0 < X < 0.5 - \varepsilon/2 \\ -1, & \text{for } 0.5 - \varepsilon/2 \leqslant X \leqslant 0.5 + \varepsilon/2 \\ 0, & \text{for } 0.5 + \varepsilon/2 < X < 1 \end{cases}$$

Right and left wall:

$$U = V = 0, \qquad \theta = 0.$$

The condition $\partial\theta/\partial Y = -1$ for $0.5 - \varepsilon/2 \leqslant X \leqslant 0.5 + \varepsilon/2$ at the bottom wall arises as a consequence of constant heat flux q'' boundary condition. Also the dimensionless heat flux at the bottom wall is $q^{*\prime\prime} = -k^*(\partial\theta/\partial Y)_{\text{wall}} = -(1/Pr)(-1) = 1/Pr$, where $k^* = 1/Pr$ is the non-dimensional thermal conductivity from Eq. (4).

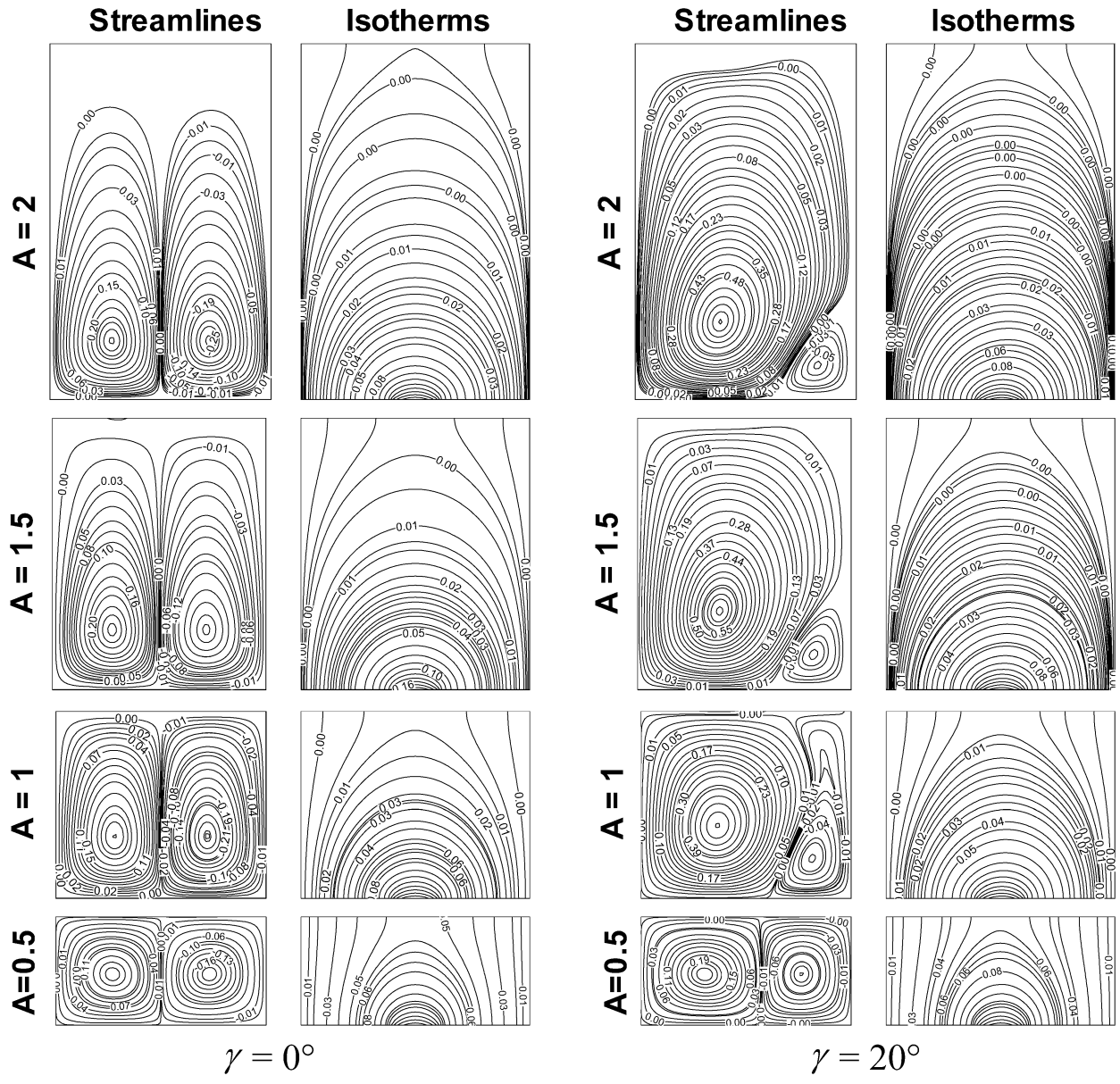

Fig. 3. Streamlines and isotherms in the cavity with $\varepsilon = 0.2$ and $Gr = 10^4$.

We define the local heat transfer coefficient $h_x = q''/[T_s(x) - T_c]$ at a given point on the heat source surface where $T_s(x)$ is the local temperature on the surface. Accordingly the local Nusselt number and the average or overall Nusselt number can be obtained respectively as

$$Nu = \frac{h_x W}{k} = \frac{1}{\theta_s(X)} \quad \text{and}$$

$$\overline{Nu} = \frac{\bar{h} W}{k} = \frac{1}{\varepsilon} \int_0^{\varepsilon} \frac{1}{\theta_s(X)} \mathrm{d}X \tag{5}$$

where $\theta_s(X)$ is the local dimensionless temperature. The trapezoidal rule is used for numerical integration to obtain the overall Nusselt number.

3. Numerical procedure

The set of governing equations are integrated over the control volumes, which produces a set of algebraic equations. The PISO algorithm developed by Issa [15] and Issa et al. [16] is used to solve the coupled system of governing equations. The set of algebraic equations are solved sequentially by ADI method. A second-order upwind differencing scheme is used for the formulation of the convection contribution to the coefficients in the finite-volume equations. Central differencing is used to discretize the diffusion terms. The computation is terminated when all of the residuals get below 10^{-5}. The calculations are done using the CFD2000 commercial code where the temperature source term in the momentum equation is incorporated through user subroutines.

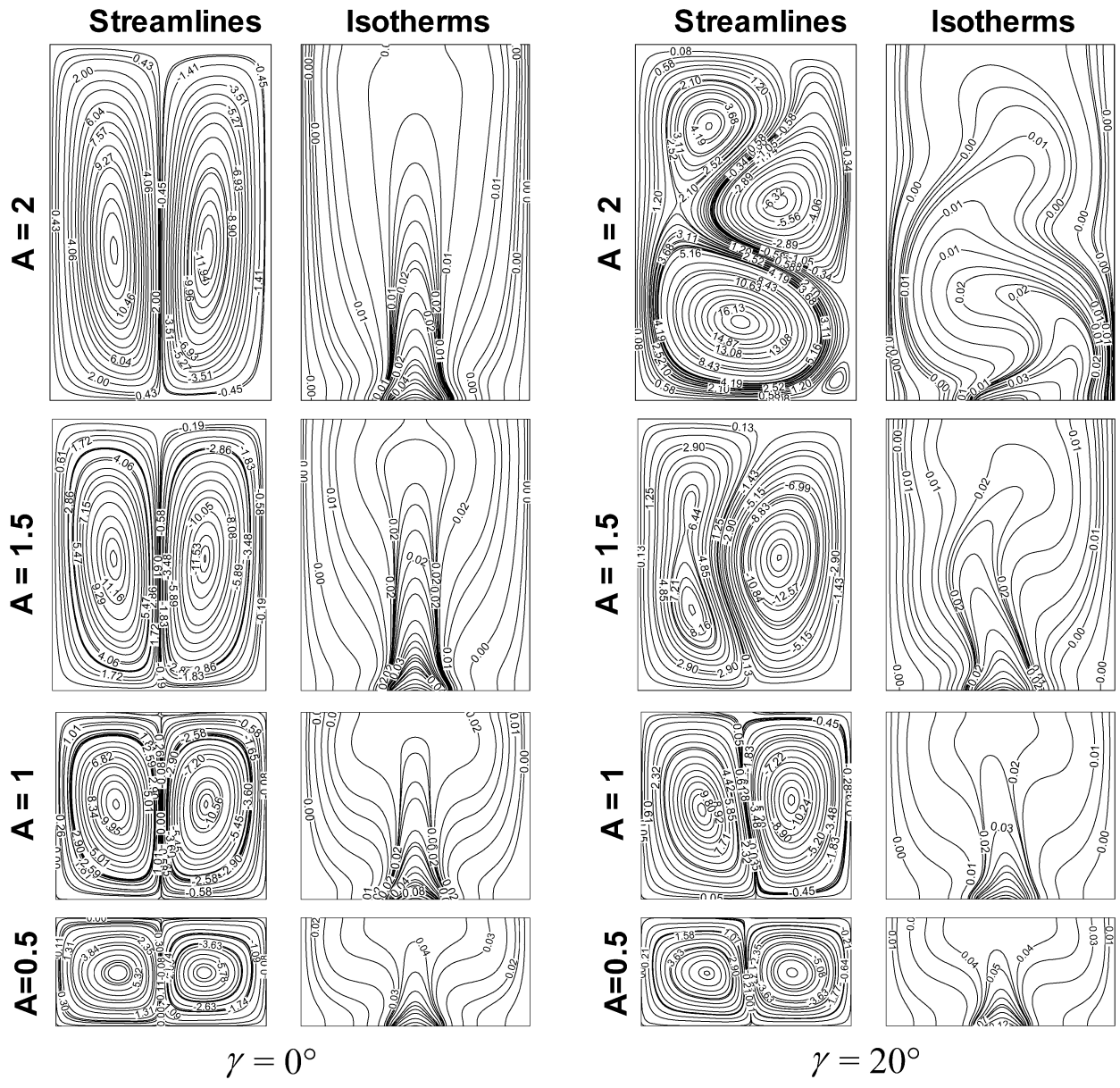

Fig. 4. Streamlines and isotherms in the cavity with $\varepsilon = 0.2$ and $Gr = 10^6$.

4. Results and discussion

The working fluid is chosen as air with Prandtl number, $Pr = 0.71$. The normalized length of the constant flux heat source at the bottom wall, ε, was varied to be 0.2, 0.4, 0.6, and 0.8. For each value of ε, the Grashof number, Gr, was varied as 10^3, 10^4, 10^5, and 10^6, the aspect ratio, A, was varied as 0.5, 1, 1.5, and 2 while the inclination angle, γ, was varied as 0°, 10°, 20°, and 30°. Thus the computations were done for a total of 256 configurations.

In order to obtain grid independent solution, a grid refinement study is performed for a square horizontal cavity ($A = 1$, $\gamma = 0$) with $\varepsilon = 0.4$. Fig. 2(a) shows the convergence of the average Nusselt number, $\overline{Nu}$, at the heated surface with grid refinement. It is observed that grid independence is achieved with a 70×70 grid beyond which there is insignificant change in $\overline{Nu}$. This grid resolution is therefore used for all subsequent computations for $A \leqslant 1$. For taller cavities with $A > 1$, a proportionately larger number of grids in the y-direction are used while keeping the number of grids in the x-direction fixed at 70.

Published experimental data are not available for the cavity configuration and boundary conditions similar to that undertaken in the present study. Thus, direct validation of the computations against suitable experimental data could not be performed. However, in order to validate the predictive capability and accuracy of the present code, computations are performed using the configuration and boundary conditions of the experiment conducted by Elsherbiny et al. [9]. They measured natural convection heat transfer in vertical

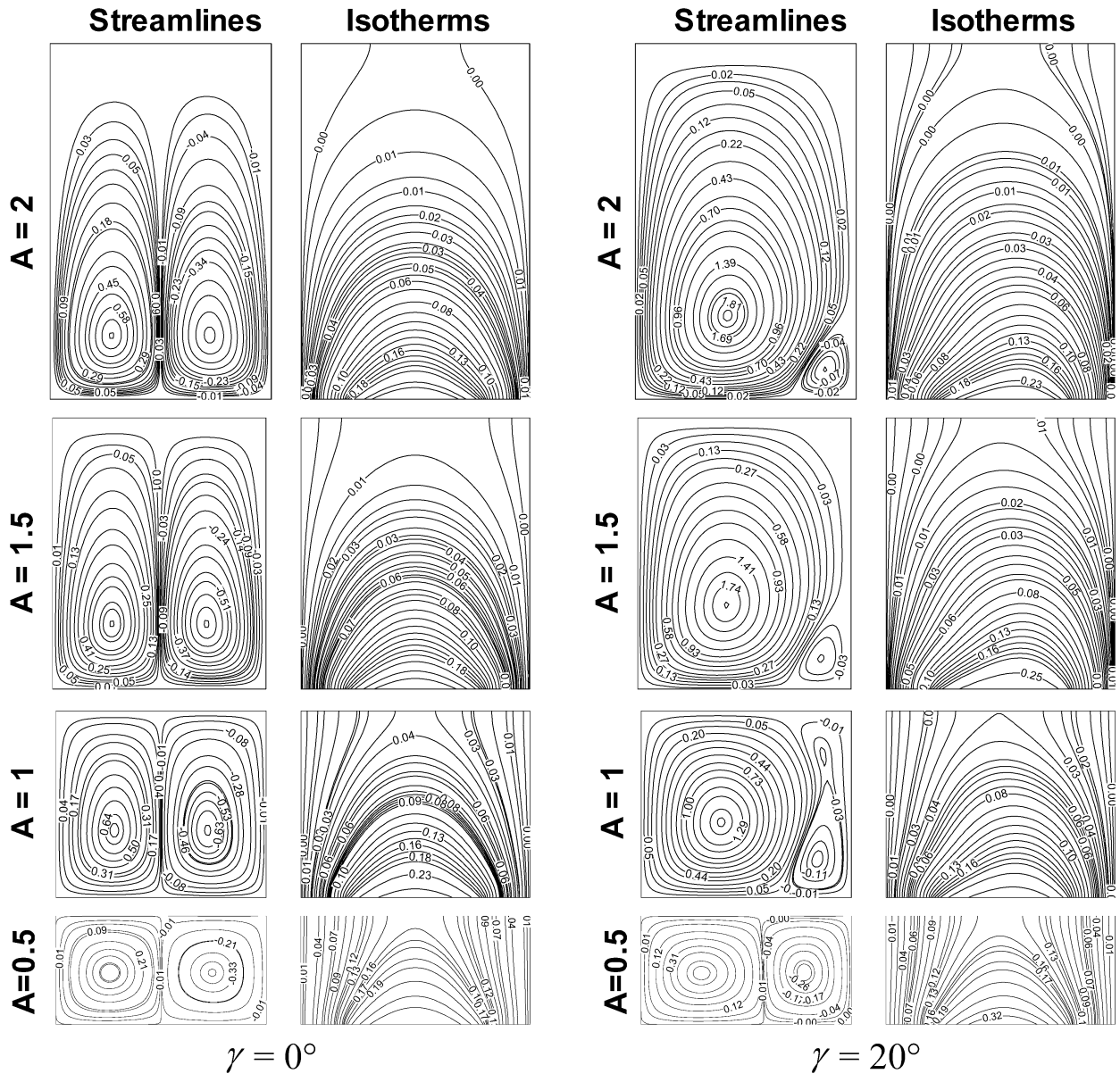

Fig. 5. Streamlines and isotherms in the cavity with $\varepsilon = 0.6$ and $Gr = 10^4$.

and inclined rectangular cavities where the isothermal sidewalls were at different temperatures and the end walls were perfectly conducting having a linearly varying temperature bounded by the temperature of the sidewalls. Computations are performed for one of their vertical cavity configuration with aspect ratio 5 for which they provided the correlation for the overall Nusselt number as a function of the Rayleigh number, Ra ($Ra = Gr\,Pr$), as

$$\overline{Nu} = \max\left\{\left[1 + \left(\frac{0.193Ra^{1/4}}{1 + (1800/Ra)^{1.289}}\right)^3\right]^{1/3}, \; 0.0605Ra^{1/3}\right\} \tag{6}$$

for $Ra < 10^8$. The average Nusselt numbers computed by the present code for values of Ra ranging from 10^3 to 10^6 are compared with the correlation of Elsherbiny et al. [9] given in Eq. (6) in Fig. 2(b). The agreement is found to be excellent with a maximum discrepancy of about 4%, which validates the present computations indirectly.

The predicted values of the average Nusselt number and the maximum temperature at the heated surface and its location for the whole set of 256 configurations computed in this study have been tabulated in Tables 1–4.

The hydrodynamic and thermal fields in the cavity in the form of streamlines and isotherms for various cavity aspect ratios are shown in Figs. 3–6 for inclination angles 0° and 20° with $\varepsilon = 0.2$ as well as 0.6, at a Grashof number of 10^4 and 10^6 as representative cases. For horizontal cavity ($\gamma = 0°$), where the buoyancy force is acting only in the y-direction, the flow domain and boundary conditions are

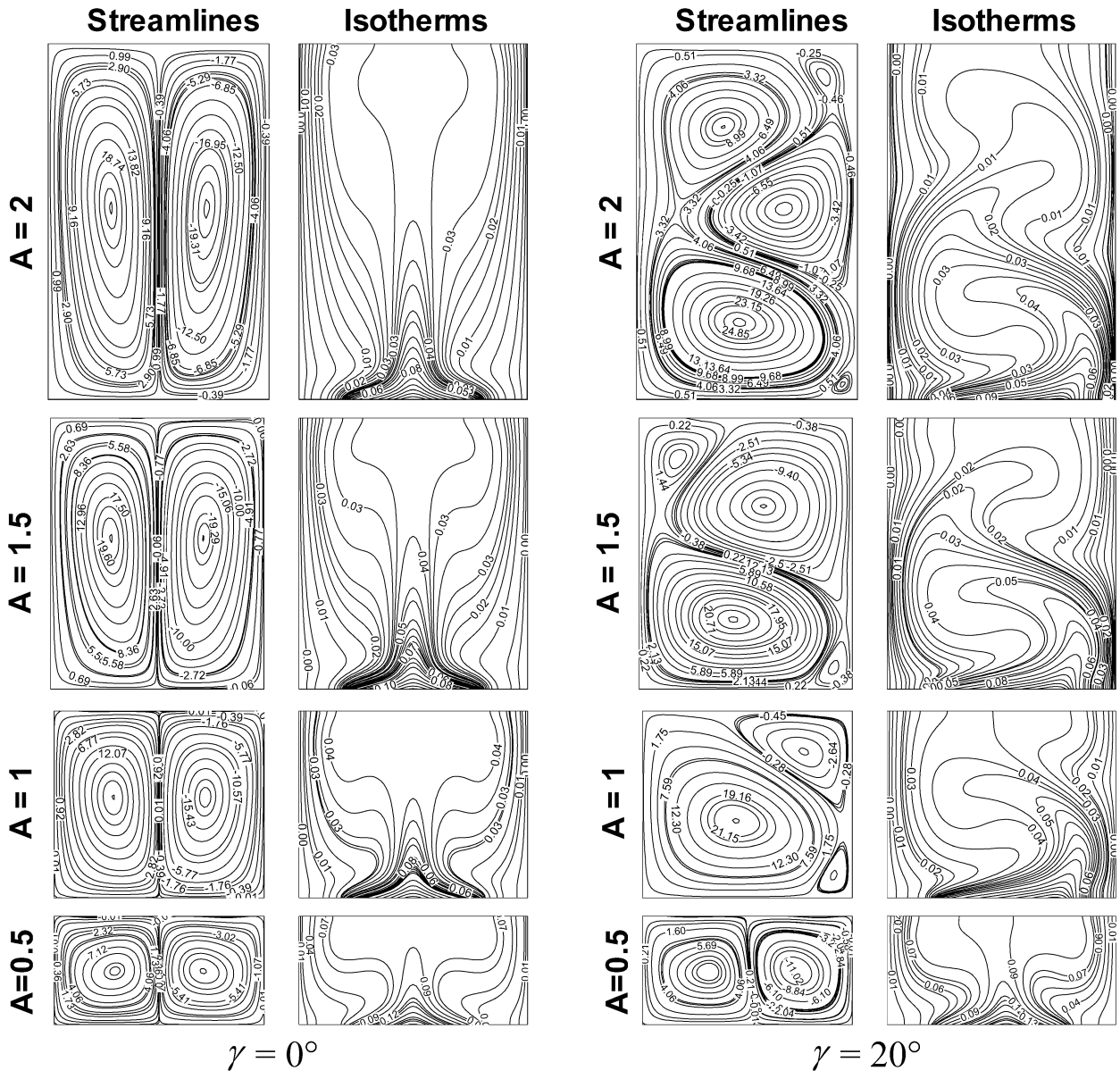

Fig. 6. Streamlines and isotherms in the cavity with $\varepsilon = 0.6$ and $Gr = 10^6$.

symmetrical and two counter-rotating rolls are formed in the cavity. In each case the flow rises along the vertical symmetry axis and gets blocked at the top adiabatic wall, which turns the flow horizontally towards the isothermal cold walls. The flow then descends downwards along the sidewalls and turns back horizontally to the central region after hitting the bottom wall. The presence of the stagnation point is noticed at the midpoint of the bottom surface. The isotherm plots are also symmetrical about the vertical mid plane and concentrated towards the hot surface indicating the presence of a large temperature gradient there. For the inclined cavity this symmetry is completely destroyed due to the buoyancy force components acting in both x- and y-directions. Multiple major and minor vortices are formed in the cavity especially for $A \geqslant 1$. Similar behavior of the flow and thermal fields is observed at other Grashof numbers, heated surface lengths, and inclination angles, for which the plots are not shown here for brevity.

The evolution of the flow and thermal fields with Grashof number for a horizontal cavity of aspect ratio 1 for a representative case with $\varepsilon = 0.4$ is presented in Fig. 7(a). Two symmetric counter-rotating rolls are formed at all Grashof numbers considered here. For lower Gr (10^3 and 10^4) the convection intensity in the cavity is very weak as evident from the stream function values which are at least an order of magnitude smaller that those for $Gr = 10^5$ and 10^6. Thus viscous forces are more dominant than the buoyancy forces at lower Gr and diffusion is the principal mode of heat transfer. At higher Gr when the intensity of convection increases significantly, the core of the circulating rolls moves up and

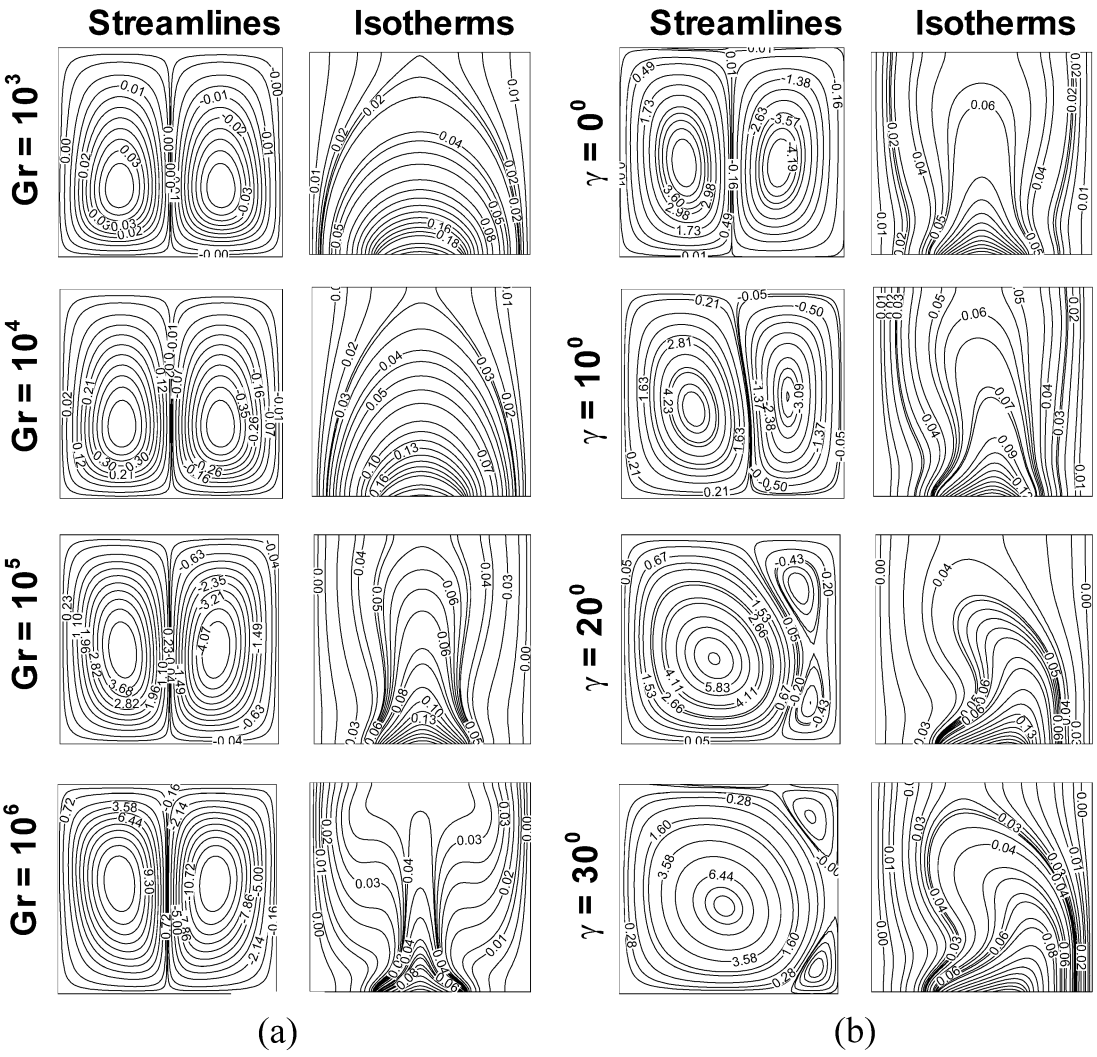

Fig. 7. Evolution of the flow in the cavity; (a) with Grashof number ($A = 1$, $\varepsilon = 0.4$, $\gamma = 0°$) and (b) with inclination ($A = 1$, $\varepsilon = 0.4$, $Gr = 10^5$).

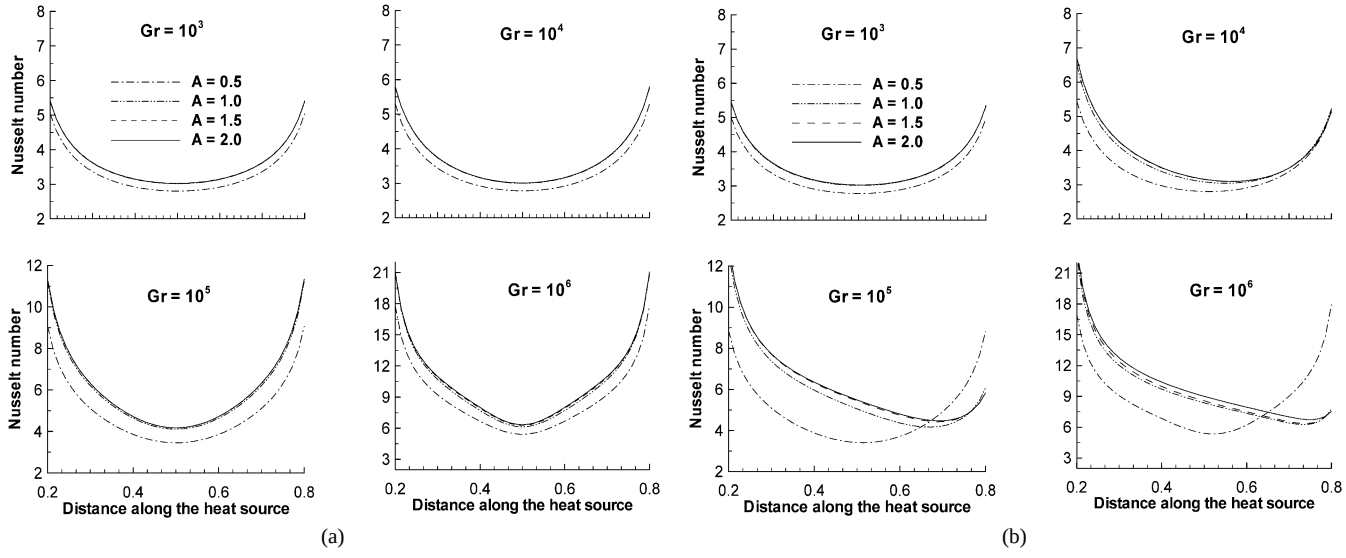

Fig. 8. Local Nusselt number along the heated surface for $\varepsilon = 0.6$; (a) $\gamma = 0°$ and (b) $\gamma = 20°$.

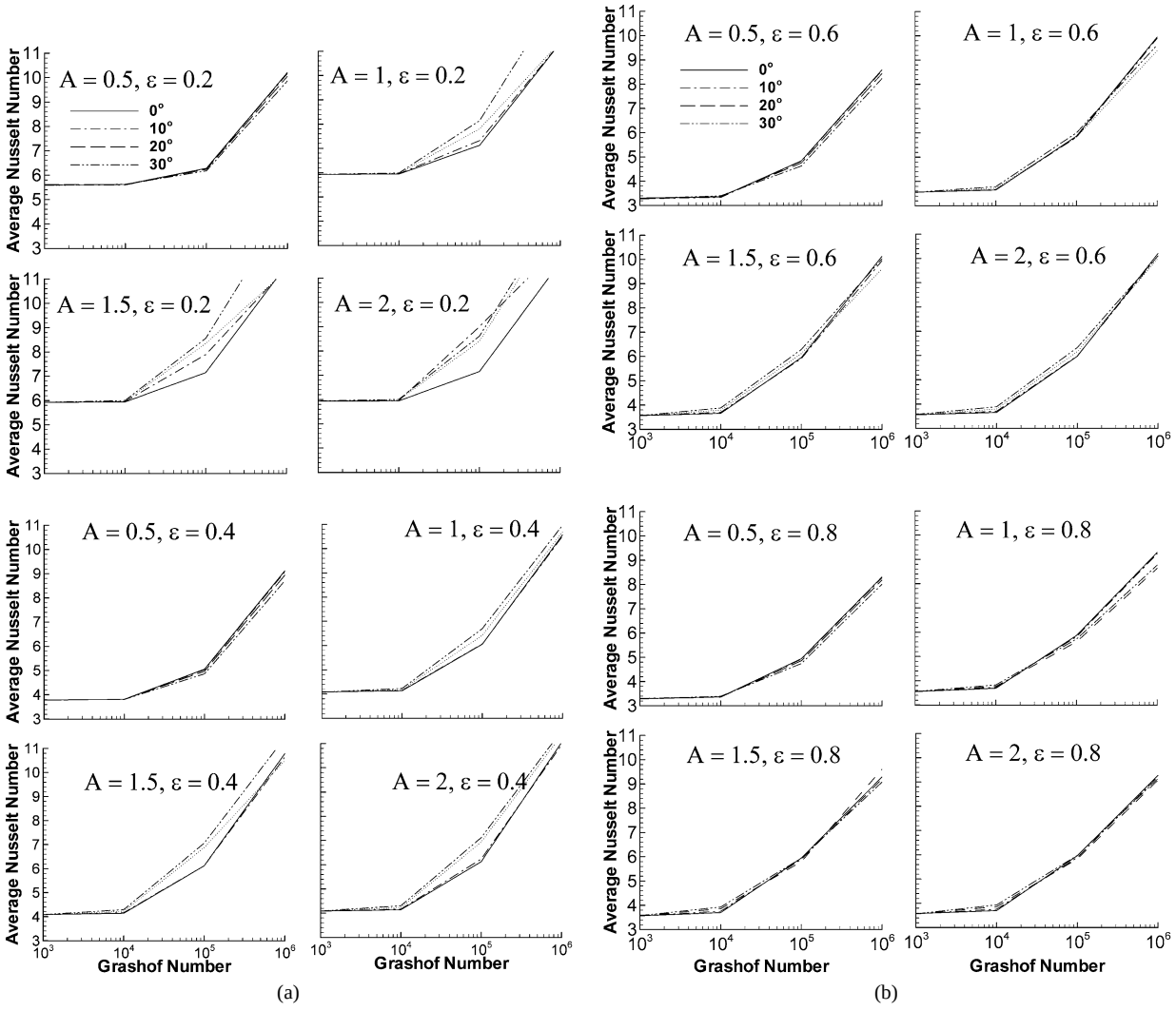

Fig. 9. Variation of the average Nusselt number at the heated surface with Grashof number.

the isotherm patterns changes significantly indicating that the convection is the dominating heat transfer mechanism in the cavity. Aydin and Yang [14] also observed similar behaviour when investigating the same problem with localized symmetrical isothermal heat source at the bottom.

The evolution of the flow and thermal fields in the cavity with increasing inclination are shown in Fig. 7(b) for a representative case of aspect ratio 1 (square cavity) and at $Gr = 10^5$ with $\varepsilon = 0.4$. It is observed that the left recirculating vortex becomes dominating in the cavity while the right vortex is squeezed thinner and ultimately is divided into two minor corner vortices. The isotherms are also adjusted according to the changes in the flow field and pushed towards the lower part of the right sidewall indicating the presence of a large temperature gradient there.

The variation of the local Nusselt number, along the heated surface for different aspect ratios and Grashof number with $\varepsilon = 0.6$ (as a representative case) is shown in Fig. 8(a) for horizontal cavity. The plots exhibit a symmetric pattern of heat transfer mechanism due to the symmetry of configuration and boundary conditions. It is to be noted that the local Nusselt number does not change significantly for taller cavities for aspect ratios greater than 1. It is observed from the streamline plots that the convection is very weak in the upper parts of the taller cavities keeping most of the convective heat transfer process confined towards the lower parts of the cavity. Thus increasing the aspect ratio beyond 1 does not improve the heat transfer process appreciably. This explains the insensitivity of the Nusselt number with larger aspect ratios at a particular Grashof number. The Nusselt number is minimum at the mid-point of the heated surface since the stagnation point is located there and convective heat transfer is minimum. The corresponding variation of the local Nusselt number for the inclined cavity at an inclination of 20° is shown in Fig. 8(b). As expected the local Nusselt number variation is asymmetric which is more prevalent at higher Grashof number and for taller cavities. In this case also the variation curves for taller cavities are clustered together with that for square cavity indicating the insensitivity of the Nusselt number with aspect ratio for taller cavities.

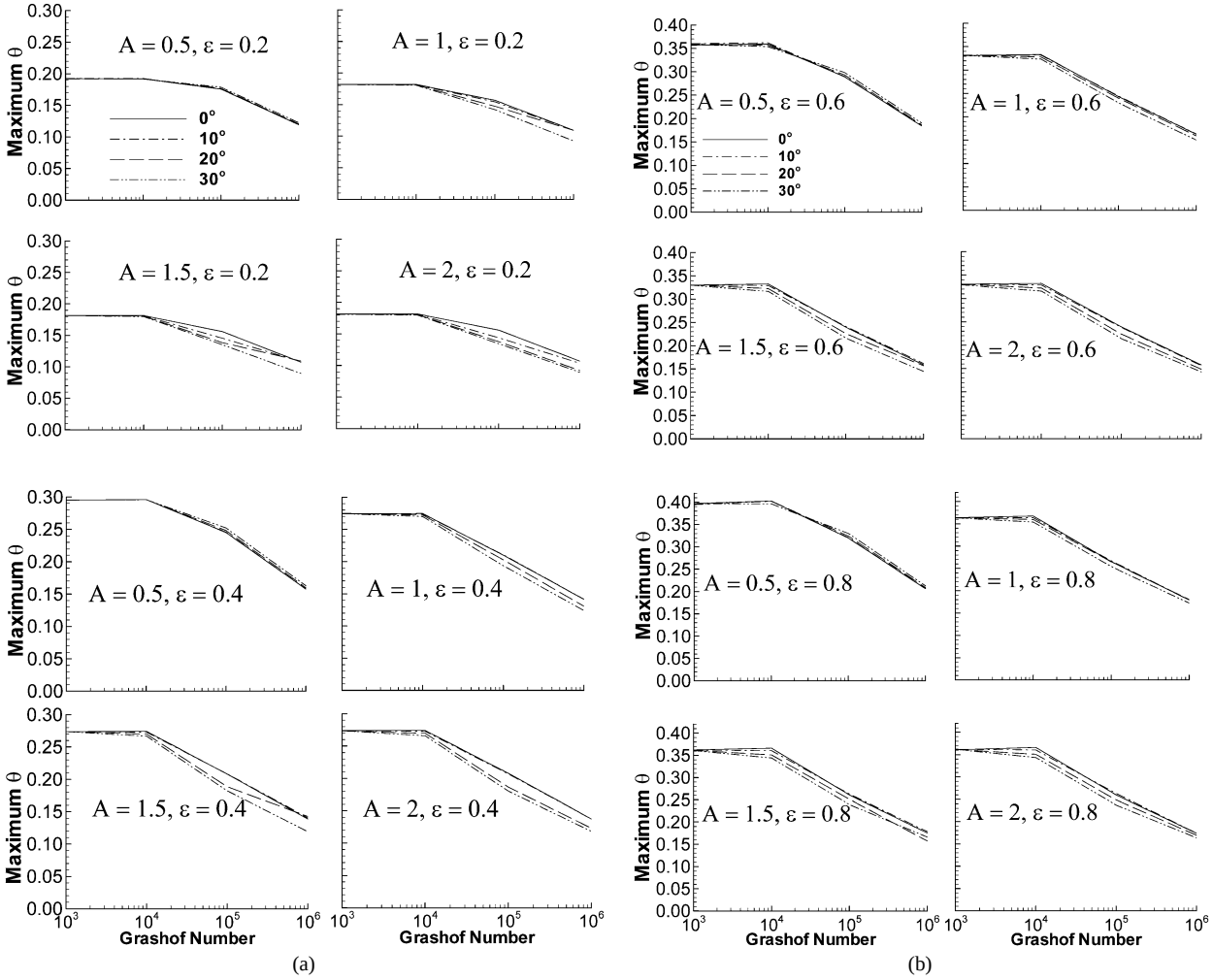

Fig. 10. Variation of the maximum temperature at the heated surface with Grashof number.

The location of the minimum Nusselt number shifts to the right as the aspect ratio is increased.

The variation of the average Nusselt number, $\overline{Nu}$, at the constant flux hot surface with Grashof number, Gr, for the entire set of the heated surface lengths (ε), aspect ratios (A), and cavity inclination angles (γ) investigated are shown in Fig. 9. In general, it is observed that at any particular aspect ratio and heat source length, $\overline{Nu}$ increases significantly with Gr due to enhanced convection especially for $Gr > 10^4$. For $Gr \leqslant 10^4$, $\overline{Nu}$ is almost invariant due to the diffusion dominated heat transfer, as mentioned earlier. Inclination has noticeable effect only for cavities with higher aspect ratios ($A \geqslant 1$) and lower heat source lengths ($\varepsilon \leqslant 0.4$).

One of the major differences between the isothermal and constant flux heat source condition is that the surface temperature at the source is not uniform and a maximum temperature exists on the surface for the latter case. In electronic component cooling applications, the maximum temperature on the surface is a critical issue since it may be detrimental to the circuitry if too high. It is therefore of interest to examine the maximum temperature at the heated surface closely. The variation of the maximum dimensionless temperature, $\theta_{\max}$, on the heated surface, with Gr for all the cases considered here is presented in Fig. 10. In general, $\theta_{\max}$ decreases with increasing Gr as opposed to the variation of $\overline{Nu}$ with Gr. This is due to the fact that the local Nusselt number is reciprocal of the dimensionless surface temperature for the constant heat flux condition. The maximum temperature decreases much more rapidly for $Gr > 10^4$ due to stronger convection. The location of $\theta_{\max}$ is at the middle of the heated surface (stagnation point) for horizontal cavity and shifts gradually to the right with increasing inclination (see Tables 1–4).

The variation of the average Nusselt number at the heated surface with aspect ratio, heat source length, and cavity inclination are shown in Fig. 11(a)–(c), respectively, for some representative cases. It is observed that while $\overline{Nu}$ increases mildly with A for a particular set of ε and γ, and decreases mildly with ε for a particular set of A and γ, it remains almost invariant with γ for a particular set of A and ε, at all Gr. It is also noticed that there is no significant difference in the variation patterns for $\overline{Nu}$ between $Gr = 10^3$ and 10^4 due to diffusion dominated heat transfer.

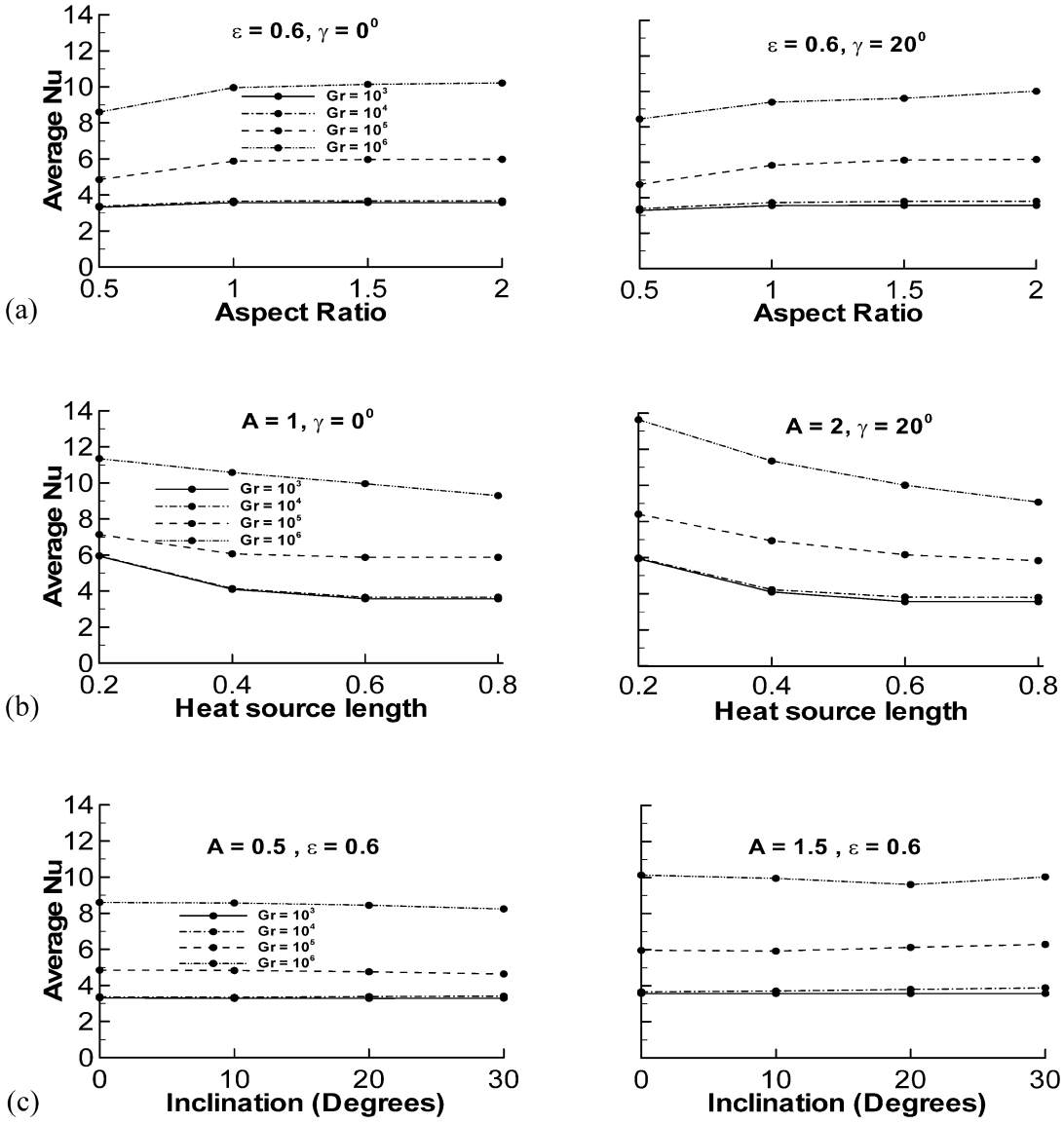

Fig. 11. Variation of the average Nusselt number, $\overline{Nu}$; (a) with aspect ratio, A, (b) with length of the heated surface, ε, and (c) with inclination, γ.

5. Conclusions

Natural convective cooling of a localized constant heat flux surface embedded symmetrically at the bottom of an air-filled rectangular cavity where the top wall is adiabatic and cold sidewalls are isothermal is investigated and analyzed numerically for a range of heat source length, Grashof number, cavity aspect ratio, and inclination of the cavity. The flow and thermal fields and the variation of the average Nusselt number and maximum temperature on the heated surface are presented for several representative cases out of the 256 configurations studied. The conclusions of the study are as follows:

(1) At lower Grashof number ($Gr \leqslant 10^4$), diffusion is the dominating heat transfer mechanism whereas at higher Grashof numbers ($Gr = 10^5$ and 10^6) buoyancy driven convection is dominating. As a result, the average Nusselt number at the heated surface does not change significantly for the diffusion dominated case whereas it increases rather rapidly with Gr for the convection dominated case.

(2) The maximum temperature at the heated surface also does not change significantly for the diffusion dominated cases but decreases rapidly with Gr for convection dominated case.

(3) The average Nusselt number and at the heated surface do not change substantially with inclination for diffusion dominated cases ($Gr \leqslant 10^4$). Inclination has noticeable effect only for cavities with higher aspect ratios ($A \geqslant 1$) and lower heat source lengths ($\varepsilon \leqslant 0.4$) for convection dominated cases ($Gr > 10^4$).

(4) The average Nusselt number and maximum temperature change mildly with aspect ratio as well as with heat source length.

Table 1
Average Nusselt number and maximum temperature and its location on the heated surface

Dimensionless heat source length, $\varepsilon = 0.2$					
Aspect ratio, A	Grashof number, Gr	Inclination angle, γ			
		0°	10°	20°	30°
0.5	10^3	5.599576 0.19219 (0.500)	5.595655 0.19232 (0.500)	5.619158 0.19155 (0.500)	5.589631 0.19251 (0.500)
	10^4	5.620137 0.19186 (0.500)	5.600419 0.19249 (0.500)	5.610877 0.19213 (0.500)	5.627235 0.19157 (0.500)
	10^5	6.287787 0.17575 (0.500)	6.272770 0.17606 (0.500)	6.240290 0.17688 (0.514)	6.180417 0.17867 (0.514)
	10^6	10.20755 0.11916 (0.500)	10.16859 0.11942 (0.500)	10.05059 0.12034 (0.514)	9.857761 0.12238(0.514)
1.0	10^3	5.926608 0.18194 (0.500)	5.926616 0.18194 (0.500)	5.926764 0.18193 (0.500)	5.933348 0.18174 (0.500)
	10^4	5.946352 0.18176 (0.500)	5.958288 0.18140 (0.500)	5.969487 0.18105 (0.500)	5.985846 0.18059 (0.514)
	10^5	7.124055 0.15682 (0.500)	7.317048 0.15443 (0.528)	7.805869 0.14737 (0.542)	8.142054 0.14202 (0.542)
	10^6	11.34151 0.10920 (0.500)	11.34926 0.10918 (0.514)	11.37748 0.10917 (0.528)	13.42033 0.09245 (0.557)
1.5	10^3	5.928022 0.18158 (0.500)	5.928479 0.18157 (0.500)	5.932820 0.18145 (0.500)	5.928059 0.18158 (0.500)
	10^4	5.942938 0.18154 (0.500)	5.955989 0.18115 (0.500)	5.970616 0.18071 (0.500)	6.001601 0.17992 (0.514)
	10^5	7.147532 0.15607 (0.500)	7.890534 0.14550 (0.542)	8.346095 0.13845 (0.542)	8.559571 0.13515 (0.542)
	10^6	11.57153 0.10728 (0.500)	11.45313 0.10811 (0.500)	11.35803 0.10909 (0.514)	13.90140 0.08958 (0.571)
2.0	10^3	5.929290 0.18159 (0.500)	5.943320 0.18118 (0.500)	5.939748 0.18128 (0.500)	5.944537 0.18115 (0.500)
	10^4	5.946185 0.18149 (0.500)	5.958255 0.18113 (0.500)	5.981195 0.18045 (0.500)	6.007791 0.17979 (0.514)
	10^5	7.150565 0.15604 (0.500)	8.000677 0.14376 (0.542)	8.399665 0.13759 (0.542)	8.612411 0.13433 (0.542)
	10^6	11.64709 0.10677 (0.500)	12.32789 0.10337(0.526)	13.63193 0.09197 (0.571)	13.94560 0.08923 (0.571)

Table 2
Average Nusselt number and maximum temperature and its location on the heated surface

Dimensionless heat source length, $\varepsilon = 0.4$					
Aspect ratio, A	Grashof number, Gr	Inclination angle, γ			
		0°	10°	20°	30°
0.5	10^3	3.782206 0.29513 (0.500)	3.782193 0.29512 (0.500)	3.782164 0.29511 (0.500)	3.782118 0.29509 (0.500)
	10^4	3.810682 0.29606 (0.500)	3.810449 0.29601 (0.500)	3.809880 0.29588 (0.513)	3.809091 0.29581 (0.513)
	10^5	5.057084 0.24507 (0.500)	5.036276 0.24568 (0.500)	4.973167 0.24808 (0.513)	4.865728 0.25203 (0.522)
	10^6	9.123732 0.15761 (0.500)	9.079546 0.15799 (0.513)	8.943295 0.15978(0.513)	8.704346 0.16281(0.522)
1.0	10^3	4.084653 0.27399 (0.500)	4.076164 0.27454 (0.500)	4.076872 0.27447 (0.500)	4.076910 0.27444 (0.500)
	10^4	4.132314 0.27458 (0.500)	4.147985 0.27380 (0.513)	4.179976 0.27234 (0.526)	4.228079 0.26996 (0.540)
	10^5	6.057670 0.20988 (0.500)	6.067433 0.21045 (0.540)	6.425491 0.20268 (0.606)	6.701919 0.19348 (0.620)
	10^6	10.57224 0.14147 (0.500)	10.52246 0.14153 (0.513)	10.69155 0.13069 (0.660)	10.97177 0.12389 (0.660)

Table 2 (*continued*)

Dimensionless heat source length, $\varepsilon = 0.4$					
Aspect ratio, A	Grashof number, Gr	Inclination angle, γ			
		0°	10°	20°	30°
1.5	10^3	4.084496 0.27376 (0.500)	4.084615 0.27375 (0.500)	4.084965 0.27371 (0.500)	4.085507 0.27365 (0.500)
	10^4	4.137095 0.27403 (0.500)	4.161966 0.27279 (0.513)	4.221478 0.26989 (0.526)	4.289744 0.26662 (0.540)
	10^5	6.118622 0.20799 (0.500)	6.122164 0.20841 (0.526)	6.874618 0.18854 (0.620)	7.060112 0.18220 (0.633)
	10^6	10.78857 0.13854 (0.526)	10.64294 0.14042 (0.486)	10.49641 0.14263 (0.513)	11.44957 0.11911 (0.660)
2.0	10^3	4.085704 0.27372 (0.500)	4.085838 0.27370 (0.500)	4.094634 0.27312 (0.500)	4.086733 0.27360 (0.500)
	10^4	4.138167 0.27399 (0.500)	4.163838 0.27271 (0.513)	4.226330 0.26963 (0.526)	4.304750 0.26575 (0.540)
	10^5	6.125487 0.20781 (0.500)	6.233948 0.20683 (0.566)	6.933184 0.18645 (0.620)	7.115624 0.18026 (0.633)
	10^6	11.03852 0.13706 (0.500)	10.93634 0.13711 (0.526)	11.34760 0.12283 (0.660)	11.51980 0.11805 (0.660)

Table 3
Average Nusselt number and maximum temperature and its location on the heated surface

Dimensionless heat source length, $\varepsilon = 0.6$					
Aspect ratio, A	Grashof number, Gr	Inclination angle, γ			
		0°	10°	20°	30°
0.5	10^3	3.306122 0.35670 (0.500)	3.275238 0.36011 (0.500)	3.275148 0.36008 (0.500)	3.289168 0.35845 (0.500)
	10^4	3.359769 0.35957 (0.500)	3.335363 0.36217 (0.500)	3.377542 0.35698 (0.514)	3.399916 0.35383 (0.514)
	10^5	4.843349 0.28933 (0.500)	4.822947 0.29003 (0.500)	4.751560 0.29327 (0.514)	4.630529 0.29845 (0.528)
	10^6	8.594213 0.18469 (0.500)	8.563475 0.18514 (0.514)	8.439362 0.18705(0.514)	8.233562 0.19090(0.528)
1.0	10^3	3.555848 0.33127 (0.500)	3.551142 0.33171 (0.500)	3.550651 0.33170 (0.500)	3.551626 0.33153 (0.500)
	10^4	3.647968 0.33342 (0.500)	3.667823 0.33209 (0.528)	3.721368 0.32824 (0.550)	3.786017 0.32359 (0.571)
	10^5	5.864100 0.24325 (0.500)	5.822127 0.24436 (0.542)	5.826853 0.23985 (0.671)	6.003543 0.22992 (0.700)
	10^6	9.949690 0.16308 (0.500)	9.900074 0.16354 (0.528)	9.388788 0.15940 (0.728)	9.624811 0.15058 (0.757)
1.5	10^3	3.564833 0.33017 (0.500)	3.563124 0.33032 (0.500)	3.560210 0.33054 (0.500)	3.564169 0.33011 (0.514)
	10^4	3.654667 0.33255 (0.500)	3.700389 0.32923 (0.542)	3.791007 0.32287 (0.557)	3.878768 0.31668 (0.585)
	10^5	5.957710 0.23973 (0.500)	5.915095 0.24124 (0.528)	6.120661 0.22584 (0.685)	6.287451 0.21651 (0.700)
	10^6	10.13065 0.15923 (0.500)	9.947491 0.16187 (0.471)	9.607379 0.15715 (0.742)	10.02722 0.14478 (0.757)
2.0	10^3	3.560450 0.33062 (0.500)	3.560647 0.33058 (0.500)	3.561853 0.33042 (0.500)	3.573636 0.32924 (0.514)
	10^4	3.655994 0.33244 (0.500)	3.705599 0.32881 (0.542)	3.796317 0.32247 (0.557)	3.889859 0.31584 (0.585)
	10^5	5.970662 0.23928 (0.500)	5.986336 0.23800 (0.585)	6.158870 0.22364 (0.685)	6.328609 0.21421 (0.700)
	10^6	10.20651 0.15779 (0.500)	10.11441 0.15623 (0.614)	10.00611 0.14865 (0.742)	10.10435 0.14285 (0.757)

Table 4
Average Nusselt number and maximum temperature and its location on the heated surface

Dimensionless heat source length, $\varepsilon = 0.8$					
Aspect ratio, A	Grashof number, Gr	Inclination angle, γ			
		0°	10°	20°	30°
0.5	10^3	3.293710 0.39652 (0.500)	3.308650 0.39447 (0.500)	3.289686 0.39696 (0.500)	3.289783 0.39683 (0.500)
	10^4	3.368128 0.40262 (0.500)	3.368647 0.40215 (0.500)	3.359017 0.40269 (0.514)	3.393484 0.39623 (0.528)
	10^5	4.942136 0.32009 (0.500)	4.921653 0.32098 (0.500)	4.858525 0.32431 (0.514)	4.741324 0.33034 (0.528)
	10^6	8.312102 0.20632 (0.500)	8.280733 0.20696 (0.514)	8.184567 0.20902(0.528)	8.013199 0.21291(0.542)
1.0	10^3	3.556180 0.36373 (0.500)	3.561278 0.36311 (0.500)	3.556242 0.36361 (0.500)	3.557804 0.36335 (0.514)
	10^4	3.691916 0.36740 (0.500)	3.724995 0.36384 (0.542)	3.768441 0.35986 (0.571)	3.826308 0.35397 (0.585)
	10^5	5.864436 0.26514 (0.500)	5.815814 0.26676 (0.542)	5.602748 0.26473 (0.714)	5.715181 0.25406 (0.742)
	10^6	9.287972 0.17925 (0.500)	9.235440 0.17989 (0.542)	8.63273 0.18037 (0.785)	8.762286 0.17223 (0.814)
1.5	10^3	3.564219 0.36242 (0.500)	3.568658 0.36187 (0.500)	3.571134 0.36149 (0.514)	3.574729 0.36104 (0.514)
	10^4	3.697599 0.36638 (0.500)	3.754360 0.36079 (0.557)	3.856081 0.35098 (0.585)	3.927922 0.34416 (0.600)
	10^5	5.947177 0.26077 (0.500)	5.897275 0.26301 (0.528)	5.800874 0.25115 (0.728)	5.943489 0.23925 (0.757)
	10^6	9.287915 0.17516 (0.557)	9.204561 0.17818 (0.471)	9.607379 0.15715 (0.742)	9.075066 0.16604 (0.828)
2.0	10^3	3.577598 0.36091 (0.500)	3.566193 0.36221 (0.500)	3.569680 0.36172 (0.514)	3.566681 0.36202 (0.514)
	10^4	3.698296 0.36633 (0.500)	3.757039 0.36059 (0.557)	3.857999 0.35087 (0.585)	3.934384 0.34360 (0.614)
	10^5	5.964245 0.25996(0.500)	5.891326 0.26316 (0.514)	5.831363 0.24855 (0.728)	5.974084 0.23701 (0.757)
	10^6	9.271771 0.17373 (0.500)	9.218151 0.17405 (0.614)	9.074269 0.16936 (0.814)	9.144006 0.16367 (0.828)

References

[1] F.P. Incropera, Convection heat transfer in electronic equipment cooling, J. Heat Transfer 110 (1988) 1097–1111.
[2] S. Ostrach, Natural convection in enclosures, J. Heat Transfer 110 (1988) 1175–1190.
[3] A. Valencia, R.L. Frederick, Heat transfer in square cavities with partially active vertical walls, Internat. J. Heat Mass Transfer 32 (1989) 1567–1574.
[4] E.E. Selamet, V.S. Arpaci, C. Borgnakke, Simulation of laminar buoyancy driven flows in an enclosure, Numer. Heat Transfer 22 (1992) 401–420.
[5] M. Hasnaoui, E. Bilgen, P. Vasseur, Natural convection heat transfer in rectangular cavities heated from below, J. Thermophys. Heat Transfer 6 (1992) 255–264.
[6] E. Papanicolaou, S. Gopalakrishna, Natural convection in shallow, horizontal air layers encountered in electronic cooling, J. Electronic Packaging 117 (1995) 307–316.
[7] L.G. Sundstrom, S. Kimura, On laminar free convection in inclined rectangular enclosures, J. Fluid Mech. 313 (1996) 343–366.
[8] T.H. Hsu, C.K. Chen, Natural convection of micropolar fluids in a rectangular enclosure, Internat. J. Engrg. Sci. 34 (1996) 407–415.
[9] S.M. Elsherbiny, G.D. Raithby, K.G.T. Hollands, Heat transfer by natural convection across vertical and inclined air layers, J. Heat Transfer 104 (1982) 96–102.
[10] T.H. Nguyen, M. Prudhomme, Bifurcation of convection flows in a rectangular cavity subjected to uniform heat fluxes, Internat. Comm. Heat Mass Transfer 28 (2001) 23–30.
[11] R. Anderson, G. Lauriat, The horizontal natural convection boundary layer regime in a closed cavity, in: Proceedings of the Eighth International Heat Transfer Conference, vol. 4, San Francisco, CA, 1986, pp. 1453–1458.
[12] M. November, M.W. Nansteel, Natural convection in rectangular enclosures heated from below and cooled along one side, Internat. J. Heat Mass Transfer 30 (1986) 2433–2440.
[13] M.M. Ganzarolli, L.F. Milanez, Natural convection in rectangular enclosures heated from below and symmetrically cooled from the sides, Internat. J. Heat Mass Transfer 38 (1995) 1063–1073.
[14] O. Aydin, J. Yang, Natural convection in enclosures with localized heating from below and symmetrical cooling from sides, Internat. J. Numer. Methods Heat Fluid Flow 10 (2000) 518–529.
[15] R.I. Issa, Solution of the implicitly discretized fluid flow equations by operator-splitting, J. Comput. Phys. 62 (1985) 40–65.
[16] R.I. Issa, B. Ahmadi-Befrui, K.R. Beshay, A.D. Gosman, Solution of the implicitly discretized reacting flow equations by operator-splitting, J. Comput. Phys. 93 (1991) 388–410.